High-temperature stainless steel supported zeolite (MFI) membranes: preparation, module construction, and permeation experiments

Eduard R. Geus[a], Herman van Bekkum[a], Wridzer J.W. Bakker[b] and Jacob A. Moulijn[b]

[a]*Department of Organic Chemistry and Catalysis, and* [b]*Department of Chemical Technology, Delft University of Technology, Julianalaan 136, 2628 BL Delft, Netherlands*

Abstract

Continuous layers of MFI (silicalite-1; Si-rich ZSM-5) have been prepared on porous, sintered stainless steel supports. Similar metal supported MFI membranes of ~50 μm thickness have been grown within stainless steel membrane modules in order to perform (high-temperature) permeation experiments. As-synthesized layers are found to be gas-tight even for small molecules such as neon. The supported MFI layers remain thermomechanically stable upon calcination at 400°C in air to remove template ions (tetrapropylammonium). Gas permeation experiments have been performed using neon, methane, *n*-butane, and isobutane according to the Wicke–Kallenbach principle with helium as a purge gas. The sequence of the pure gas permeabilities at room temperature and 0.3 bar partial pressure difference is methane > *n*-butane > neon ≫ isobutane, demonstrating that the permeation is based on both adsorption and diffusion. The deviating permeation behaviour between the butane isomers is attributed to the bulkiness of isobutane, which is also reflected in the substantially lower adsorption capacity as compared with *n*-butane. In experiments using binary mixtures of strongly (butane isomers) and weakly (methane) adsorbing species, the permeation rate of the former is hardly affected, whereas for the latter a drop in permeability of some two orders of magnitude is observed. At higher temperatures (up to 350°C) with a constant feed composition, the methane permeation rate increases as a result of the decreased adsorption of *n*-butane. The MFI layer retains its separation potential after several heating and cooling cycles.

Keywords: ZSM-5/silicalite-1; zeolite membranes; stainless steel support, high-temperature module; permeation

Introduction

The preparation and characterization of zeolite membranes has been pursued since the early eighties, and several approaches to the preparation of inorganic zeolite membranes have been explored thus far [1–3]. Recently, several workers have reported on the preparation of unsupported MFI (ZSM-5) layers or films [4–6]. The separation potential of zeolites in a membrane configuration has been studied by performing permeation experiments on one or several zeolite crystals, embedded in epoxy resin [7–9]. Few studies, however, have been dedicated to formulate a permeation theory for single-component flow through zeolites [10,11].

Theory and practice of multicomponent flow through zeolites is even more underdeveloped.

The scientific interest in zeolite membranes is based on the generation of reliable data on intracrystalline (micropore) diffusion. Membrane permeation measurements can be performed within a very broad range of diffusivities, thus allowing for comparison of differently behaving molecules. Most other techniques are restricted to either fast or slow systems, which complicates comparison [12]. Moreover, permeation may be studied under steady state and/or transient conditions, and for both single components and mixtures. In all cases, however, the boundary conditions on either side of the membrane are well defined, which allows

for a reliable interpretation of the observed permeation behaviour.

The expected molecular sieving effect of zeolite membranes, on which the industrial interest is based, has not yet been confirmed experimentally. The permeation results for the previously mentioned zeolite crystal/epoxy resin composite membranes are not very promising, and the thus far proposed membrane preparation methods do not lead to easy scale-up. Moreover, the advantage of inorganic membranes exists in the more severe conditions (e.g., high temperature) under which such membranes can be applied and, if necessary, reactivated, as several organic polymer membranes are available with excellent performance in both permeation rate and selectivity. It is generally acknowledged that the high-temperature application of inorganic membranes is strongly limited by high-temperature resistant sealing [13]. The compatibility problem can be avoided by the application of several layers to join the ceramic membrane and the (generally) stainless steel housing [14].

Indeed, the preparation of the membrane layer or film is seldom performed in such a way that no separate incorporation within a membrane module is required [15]. Therefore, it is the objective of this work to discuss the direct membrane preparation within a high-temperature membrane module, thus avoiding the use of high-temperature resistant, gas-tight sealants. To this end, MFI layers have been grown on porous sintered stainless steel supports, which guarantees good thermomechanical compatibility between the porous support and the membrane module housing. In addition, stainless steel offers several other advantages over ceramic supports, such as (i) easy construction, (ii) mechanical strength, (iii) chemical inertness, and (iv) relatively high thermal conductivity as compared to ceramics. Some permeation measurements on the prepared MFI membranes have been included to demonstrate the interesting permeation behaviour of this new type of membrane. Finally, the use at high temperatures in connection with the thermal stability of the composite system is discussed.

Theory

Steady state membrane permeation measurements under well-defined boundary conditions offer a straightforward method to acquire accurate data on diffusion. The experimental set-up according to the Wicke–Kallenbach principle is favoured [16,17], because permeation is exclusively driven by a concentration gradient. If intracrystalline diffusion through the zeolite layer is the rate determining process for permeation, Fick's first law of diffusion applies:

$$\phi_{mol} = -D(q) \cdot A_m \cdot \frac{\partial q}{\partial x} \tag{1}$$

with ϕ_{mol} the flow rate (mol/s), $D(q)$ the concentration-dependent intracrystalline Fickian diffusivity (m²/s), q the sorbate concentration (mol/m³), A_m the membrane surface area (m²), and x the distance within the membrane layer (m).

Permeation through supported membranes, however, is affected by the presence of the support, and a more complex permeation model is required. Mainly for rather thin membranes, the membrane/support interface porosity is an essential parameter, as the effective membrane thickness is considerably larger than the actual layer thickness. For the same reason, the effective membrane surface area on either the feed (adsorption), or the permeate (desorption) side is reduced. According to Barrer [10], however, the sorption processes to and from the zeolite micropores may be considered fast as compared to intracrystalline diffusion, provided relatively thick layers (> 50 μm) are considered at room temperature. Such thick membrane layers are studied in this work, hence permeation is expected to be basically governed by intracrystalline diffusion. The extra resistance to mass flow by gas diffusion through the porous support (the zeolite layer faces the feed side) is expected to be nullified by the high flow rate of the purge gas.

Under steady state conditions the permeability (P) may be defined as a convenient parameter to relate the observed permeate flow rate to the imposed (partial) pressure difference (Δp) over the membrane:

$$\phi_{mol} = P \cdot \frac{A_m}{l_m} \cdot \Delta p \tag{2}$$

with l_m (m) the membrane thickness. Only within the Henry region, however, the permeability may

be considered constant, and defined as $P = D \cdot K$, with K the Henry coefficient (mol m^{-3} Pa^{-1}). Generally, the diffusivity is concentration dependent as in eqn. (1), and the permeability will slightly decrease for increasing feed pressures.

Equation (2) demonstrates that the permeation rate depends on both sorption and diffusion. Even for adsorption within the Henry region, stronger adsorbing molecules will experience a much larger driving force than weakly adsorbing species. Therefore, pure gas permeability ratios will generally not reflect the large differences in diffusivity, that are related to the mobility within the zeolite micropores.

The selectivity (α) is generally defined as the enrichment factor of one component in the permeate as compared to the feed composition ratio:

$$\alpha = \frac{x_F \cdot y_P}{x_P \cdot y_F} \qquad (3)$$

with $x_{F,P}$ and $y_{F,P}$ the molar fraction on the feed (F) and the permeate (P) side, respectively. Even within the Henry region, the selectivity of a binary mixture will vary with the applied conditions on both the feed and the permeate side of the membrane. This was previously demonstrated for permeation measurements on hydrogen/methane mixtures through clay supported MFI layers [18].

Outside the Henry region, the diffusivity cannot be considered equal to the intrinsic diffusivity (D_0), and it is more appropriate to take the gradient of the chemical potential ($\partial\mu/\partial x$) into account, which is the true driving force for permeation. In order to describe permeation by Fickian diffusion (purely concentration driven process), $D(q)$ is related to the intrinsic diffusivity [$D_0(q)$] by a Darken-type equation [19]:

$$D(q) = D_0(q) \cdot \frac{d \ln p}{d \ln q} \qquad (4)$$

The factor (d ln p/d ln q), generally referred to as the Darken factor [20], can be directly obtained from the adsorption isotherm. In a previous study, the steady state permeation of methane and n-butane as a function of the feed and the permeate pressure at room temperature was evaluated, assuming Langmuir-type adsorption [21]. Self-

diffusivity (PFG NMR) data [22] were used under the assumption that $D_0(q)$ could be considered equal to the self-diffusivity [$D_s(q)$]:

$$\int_0^{l_m} \phi_{mol} \cdot dx = -A_m \int_{q_F}^{q_P} D_s(q) \cdot \frac{d \ln p}{d \ln q} \cdot dq \qquad (5)$$

in which q_F and q_P denote the sorbate concentration on the feed and the permeate side, respectively, in equilibrium with the gas phase. For relatively low feed pressures (< 25 kPa) and at room temperature, the methane permeation was calculated to be proportional to the feed pressure, whereas for n-butane a strongly non-linear behaviour was found.

The Fickian diffusion model presented in eqn. (5) is strongly dependent on the Darken factor, which is directly related to the sorption model applied. It should be pointed out that the Langmuir adsorption model, from a theoretical point of view, is not valid for near saturation adsorption. On the other hand, from the shape of most adsorption isotherms (type I, according to the Brunauer classification) it is not likely that other adsorption models will lead to a very different thermodynamical correction (Darken factor) for diffusion. From these considerations, the permeation model presented in eqn. (5) may be used to relate the theoretical pure gas permeation rates to the experimental ones.

Experimental

Crystallization

Porous, sintered stainless (AISI 316) steel supports (diameter 25 mm; thickness 3 mm) were provided by Krebsöge (Radevormwald, Germany). The high-porosity supports were provided with a thin (50–150 μm) top layer of metal wool (R/F 1). For the construction of two high-temperature membrane modules, similar substrates (diameter 20 mm) were incorporated in non-porous stainless steel (AISI 316) disks (cf. Fig. 1). Intimate contact between both parts was achieved by non-isothermic assemblage (porous support at liquid nitrogen temperature; non-porous disk at 400°C).
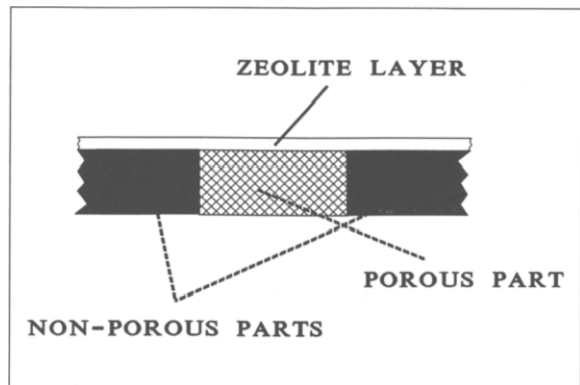
Fig. 1. Schematic view of a zeolite layer on top of a porous/non-porous substrate.

Two stainless steel cylinders, provided with commercial flange connections (Leybold–Heraeus), were subsequently connected to the non-porous part of each disk with a gold alloy. In Fig. 2 a photograph of the complete high-temperature module is shown. During hydrothermal treatment, the top section of the module (with the smooth top layer) is filled with the synthesis mixture, and the lower section is effectively closed by a Teflon cylinder (also shown in Fig. 2). Both sides of the module are closed with flange connections using Teflon sealing rings.

Prior to the formation of MFI layers within the above high-temperature modules, several hydrothermal syntheses were performed on separate porous supports within Teflon-lined (30 ml) autoclaves. In these experiments, the chemical composition of the synthesis mixture was optimized for the formation of a continuous MFI layer, fully covering the porous metal substrate. The metal disks were installed into tight-fitting Teflon holders, thus only exposing the smooth top face of the disks to the synthesis mixture.

All synthesis mixtures contained in principle only silica, tetrapropylammonium (TPA) as a template, and water. In the first experiments, gel compositions were based on the synthesis procedure according to Ghamami and Sand [23]: Ludox AS-40 (Du Pont), ammonia (25%, Baker), and TPAOH (40%, CFZ, Zaltbommel, Netherlands). In the present work, however, we will focus on more diluted synthesis mixtures at high pH (13.5–14) and higher template concentrations. In these experiments Aerosil 200 (Degussa) was used as the silicon source, and TPA was added from two sources: TPABr (CFZ), and TPAOH. The introduction of alkali atoms (Na, K) was avoided to ensure the maximal incorporation of TPA (four per unit cell) in the framework. Nevertheless, low concentrations of potassium and sodium were introduced in the synthesis mixture by the TPAOH source (1.2 wt% K; 0.04 wt% Na). For comparison, the previously applied synthesis mixture for the preparation of continuous MFI layers on ceramic supports (in the presence of sodium ions) has been tried as well [18].

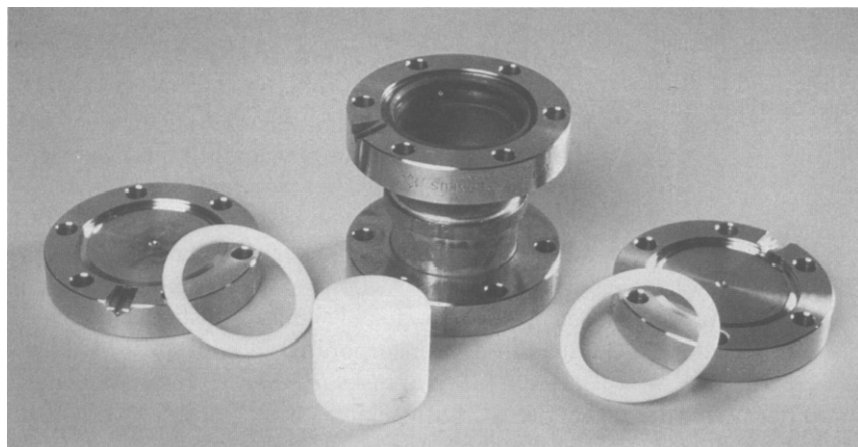All synthesis mixtures were aged while stirring

Fig. 2. Picture of the high-temperature stainless steel membrane module and Teflon sealing rings and cylinder.

for 5 h under ambient conditions. The hydrothermal synthesis was always performed at 180°C. After reaction, the metal disks were washed with water and then ethanol, and dried in air. The MFI layers were characterized by light and electron microscopy (SEM), and by X-ray diffraction. Chemical analysis by ICP and AAS was carried out on both the initial synthesis mixtures and the supernatants after hydrothermal treatment. EDAX elemental analysis was performed on an MFI/metal composite, as prepared according to the optimized synthesis procedure.

The optimized synthesis mixture was applied to prepare continuous MFI layers within the high-temperature membrane module. In addition, some blank experiments were performed within the Teflon-lined autoclaves in the absence of stainless steel, so as to study the effect of the metal substrate on the crystallization. A calcined MFI layer was subsequently removed from the membrane module by treatment with a 4 M KOH solution at 180°C for 12 h, thoroughly washed with water, and again provided with an MFI layer.

Permeation

The membrane module (with a freshly prepared MFI film) was installed in the permeation apparatus using similar flange connections as for the hydrothermal synthesis. Instead of Teflon, commercially available high-temperature resistant copper sealing rings were applied. In this configuration it was possible to flush gas through both module compartments independently. The permeation experiments were performed according to the Wicke–Kallenbach concept (concentration gradient as the driving force), using helium as a purge gas. Generally, gas flows of 100 ml (STP)/min were applied on either side of the membrane (total pressure 1 bar). The feed composition could be varied from 0.1 to 100% in helium by mass flow controllers. The permeate side was continuously flushed with helium, and analyzed by mass spectrometry (Leybold–Heraeus). In all experiments, the zeolite layer was exposed to the feed side, because the inner surface of this compartment was fully covered with MFI material. On the permeate side, this extra MFI material may influence the

transient permeation results, as the permeating molecules are readsorbed. High purity gases were used (Intermar, Netherlands): helium (99.996%), methane (99.5%), neon, n-butane, and isobutane (99.95%). The mass spectrometer was calibrated by self-made mixtures in helium within the same range as the permeate concentrations.

First, the permeability of the as-synthesized MFI layers (containing TPA) was tested for a pure neon feed (100%). In previous studies it was established that TPA-containing MFI crystals are gas-tight for all gases, even for small molecules such as hydrogen and helium [9,18,21]. Next, the MFI layer was calcined at 400°C (ramp 1°C/min; dwell 16 h) in air (100 ml/min through both compartments). In this work we only discuss the permeation experiments on membrane HTSS-2, although similar behaviour has been observed for both other membranes (HTSS-1 and HTSS-1a). On the four previously mentioned test gases both transient and steady state permeation measurements were performed at room temperature. For transient measurements the membrane module was initially flushed with pure helium until no other species were apparent by mass spectrometry (<5 ppm; 0.5 Pa). On the feed side a mixture of the permeate gas and helium was introduced, while the composition of the permeate was measured in time until steady state was reached. A delay time of approximately 26 s was found in a separately performed experiment on a membrane module without any zeolite material inside. Other transient measurements were performed by changing the feed from 70% methane to a methane/butane isomer mixture (70/30; n-butane or isobutane), and the transient permeation behaviour of an equimolar methane/n-butane mixture was studied under ambient conditions.

In order to study the effect of the macroporous stainless steel support, the steady state permeation rates for methane and neon were measured for different purge gas flow rates (on the permeate side) at room temperature. The steady state permeation behaviour of an equimolar methane/n-butane mixture (pure) was studied within the temperature region of 20–350°C by subsequently heating (1°C/min) and cooling (1.5°C/min). The thermal stability of the stainless steel supported MFI mem-

brane was checked by repeated heating and cooling (three times).

Results and discussion

Crystallization

An overview of the resulting MFI products for different gel compositions (M and SS series) is presented in Table 1, including the experiments within the membrane modules (HTSS series). Exclusively MFI material is formed, which is confirmed by XRD and light and electron microscopy. However, the nature of the MFI phase on the metal disks strongly depends on the synthesis mixture composition, and varies from separate crystals to continuous layers.

A seemingly continuous MFI layer, but in fact still containing mesopores, is obtained from the

synthesis mixture according to M-1. This has been established by applying some water on top of the dried, as-synthesized layer. In all cases, the water is readily absorbed through the deposited MFI layer into the porous metal support. In Fig. 3 a cross-sectional view of the MFI layer is shown. The layer consists of small aggregated crystals, in which some mesopores are visible. Therefore, this approach has been abandoned at an early stage. It is, however, noteworthy that unsupported MFI membranes have been grown on Teflon slabs by Tsikoyiannis and Haag [4] from a synthesis mixture with a comparable composition (100 SiO_2 : 5.2 TPABr : 4.4 NaOH : 2832 H_2O).

In contrast to the above-mentioned inhomogeneous layers, the synthesis mixture according to SS-1 (cf. Table 1) yields continuous MFI layers (Fig. 4a), and no water absorption is observed. The cross section of this layer of ~75 μm thickness is shown in Fig. 4b. Figures 5a and b present the

TABLE 1

Preparation results of the *in situ* crystallization of MFI on porous, stainless steel supports (reaction temperature 180°C)

Exp.[a]	Gel composition	Time (h)	Product
M-1[b]	100 SiO_2 : 54 NH_3 : 6 TPAOH : 6330 H_2O	58	Thick layer (100 μm), containing mesopores (Fig. 3)
SS-1	100 SiO_2 : 100 TPA : 50 OH⁻ : 10 000 H_2O	48	Continuous, polycrystalline layer (75 μm) (Figs. 4a and b)
SS-2	100 SiO_2 : 150 TPA : 50 OH⁻ : 100 000 H_2O	26	Many, small (60 μm length) crystals (Fig. 6)
SS-3	100 SiO_2 : 400 TPA : 150 OH⁻ : 26 000 H_2O	45	Near to continuous layer (Fig. 7)
SS-4	100 SiO_2 : 230 TPA : 230 OH⁻ : 25 000 H_2O	102	Intergrown crystals, partly covering the support (Fig. 8)
SS-5[c]	100 SiO_2 : 300 TPA : 300 OH⁻ : 16 667 H_2O	174	Separates large crystals (up to 400 μm length)
HTSS-1	100 SiO_2 : 100 TPA : 50 OH⁻ : 11 000 H_2O	49	Continuous, polycrystalline layer
HTSS-2	100 SiO_2 : 230 TPA : 75 OH⁻ : 14 000 H_2O	45	Continuous, polycrystalline layer
B-HTSS-2	100 SiO_2 : 230 TPA : 75 OH⁻ : 15 000 H_2O	45	Inhomogeneous, polycrystalline layer (Figs. 9a–c)
HTSS-1a	100 SiO_2 : 100 TPA : 50 OH⁻ : 9000 H_2O	36	Continuous, polycrystalline layer

[a]M and SS denote metal support in Teflon holder; HTSS denotes high temperature membrane module; B-HTSS denotes blank experiment (no metal present). [b]With Ludox AS-40 and ammonia. [c]TPABr and NaOH instead of TPAOH.
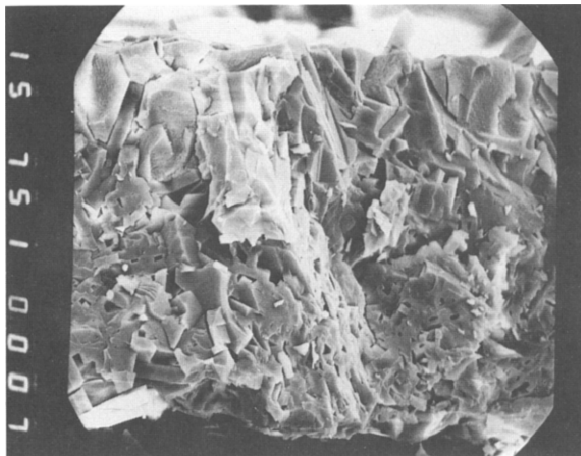
Fig. 3. SEM-picture of a cross section of the MFI layer on stainless steel, prepared according to M-1, containing meso-pores (magnification 1500 ×).

Fig. 4a. SEM picture of a continuous MFI layer (top view), prepared according to SS-1 (magnification 600 ×).

Fig. 4b. SEM picture of a cross section of the same two-layer stainless steel supported MFI layer (magnification 600 ×).

cross-sectional overview of the composite membrane by SEM and EDAX elemental image, respectively. A pure silica MFI layer (red) is supported by the blue stainless steel substrate, consisting of mainly iron, chromium, and nickel. Some small MFI crystals can be observed on the stainless steel within the wide pore section (the small red dots within the blue support). Even the thin metal top layer with substantially smaller pores has retained the greater part of its porosity. This is rationalized by the low applied silica concentration in connection with the limited hold-up of the synthesis mixture within the macropores of the support. During the crystallization process, the pores within the metal support become isolated from the bulk solution by the developing MFI layer. On the outer surface, on the other hand, the crystal growth can continue from nutrients in the bulk solution.

Unless the crystallization is favoured in a specific direction as on the extremely smooth and non-porous Si-wafers [24], total coverage of the porous support requires a relatively large layer thickness. Inevitably, the growth on a macroporous support will lead to a randomly grown crystalline layer, because the crystal growth proceeds from nuclei with a large variation in orientation. Hence, the minimal layer thickness is expected to be more or less correlated to the maximal pore 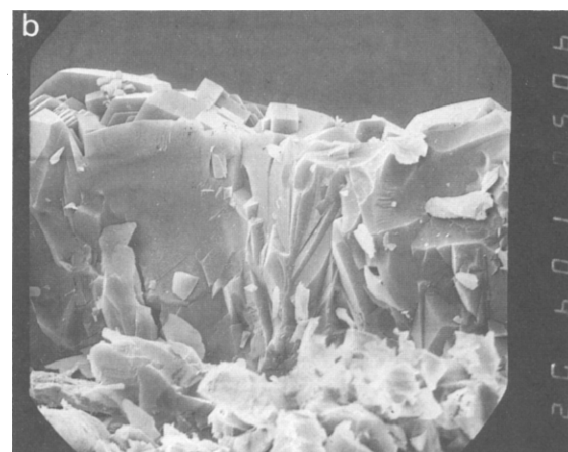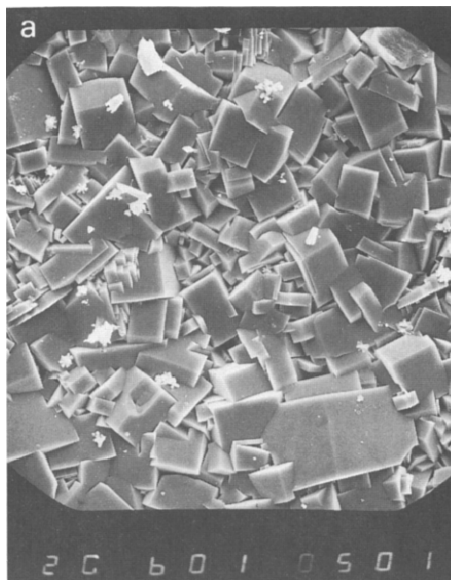size of the porous support, also depending on the smoothness of the support top face. For this reason two-layer stainless steel supports have been used, thus combining a high porosity support and a smooth top layer with a smaller pore size (~10 μm). On one-layer stainless steel supports with a comparable pore diameter, the nucleation has been found to proceed on each metal particle separately, and no continuous layers are obtained.

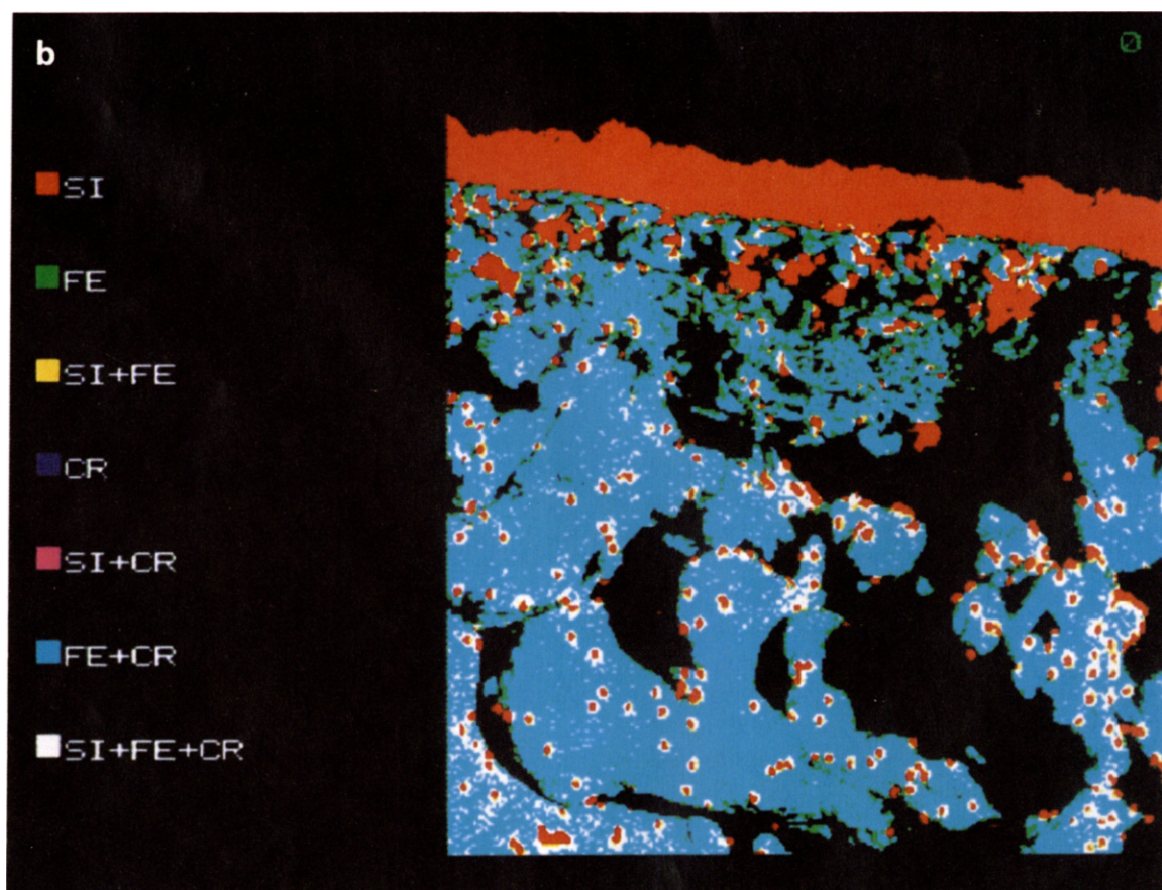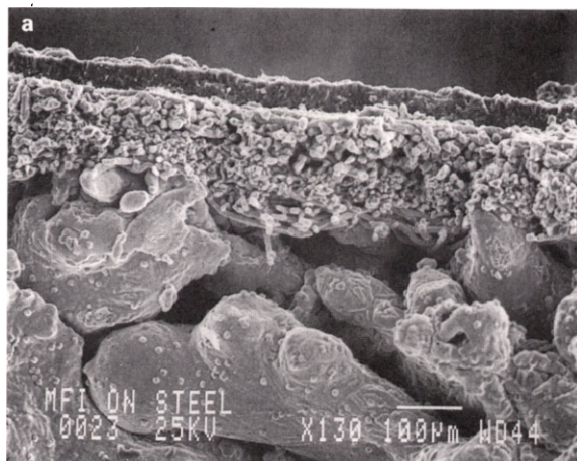The crystallization process, however, is not lim-

Fig. 5a. Cross-sectional overview (SEM) of the MFI composite membrane, prepared according to SS-1 (magnification 130 ×).

Fig. 5b. EDAX elemental image of the cross-sectional overview of the same two-layer stainless steel supported MFI membrane.

ited to the stainless steel support, and also proceeds on the exposed Teflon parts within the autoclave. In Fig. 6 the resulting MFI phase on top of the two-layer stainless steel support is shown (SS-2), prepared from a tenfold diluted mixture as compared with SS-1. If all available silica had been deposited on top of the stainless steel support, a 100 μm thick MFI layer would have yielded (surface area 5 cm^2). Instead, the support is only partly covered by thin crystals of ~60 μm length. The availability of nutrients for crystallization is further limited by the silica-to-hydroxide (SiO$_2$/OH$^-$) ratio (cf. Table 1: SS-3,4,5; Figs 7, 8). For decreasing SiO$_2$/OH$^-$ ratios, the solubility of silica is enhanced, and a substantial amount of the nutrients for crystallization remains in solution. In Table 2 the ICP and AAS chemical analyses before and after (supernatants) hydrothermal synthesis are presented for some experiments. After long synthesis times (174 h), the consumed silica (yield) for SS-5 (SiO$_2$/OH$^-$ = 0.3) is ~57%. For higher SiO$_2$/OH$^-$ ratios (0.7–2.0; SS-3,4), the yield is at least 80%, even after only 36 h. The layer thickness within the high-temperature modules can be esti-
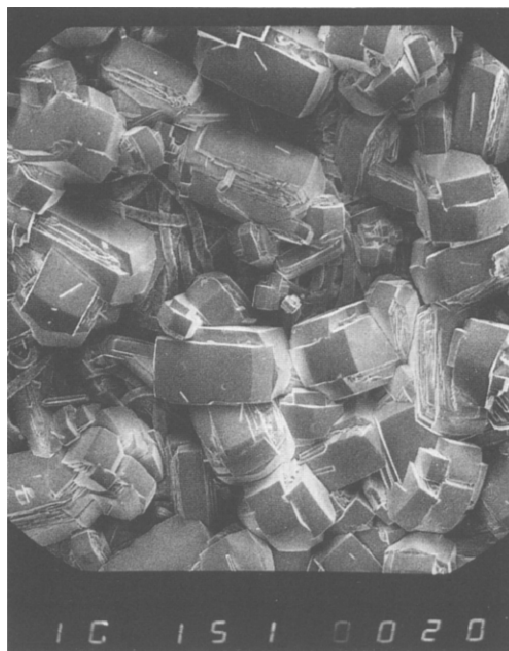

Fig. 7. SEM picture of a near to continuous MFI layer on top of a two-layer stainless steel support, prepared according to SS-3 (magnification 150 ×).

Fig. 6. SEM picture of small MFI crystals on top of a two-layer stainless steel support, prepared according to SS-2 (magnification 300 ×).

Fig. 8. SEM picture of a partly covered two-layer stainless steel support, prepared according to SS-4 (magnification 130 ×).

TABLE 2

Chemical analysis before (synthesis mixture) and after (supernatant) hydrothermal treatment (cf. Table 1)

Exp.	Si (g/kg)		SiO$_2$ deposited (g)	Yield (%)	Na (mg/kg)		K (g/kg)		pH (formal)	Leached materials
	in	out			in	out	in	out		
SS-3	4.8	1.0	0.29	79	50	60	1.6	1.8	13.5	0.03 mg Mo
SS-4	5.5	3.5	0.14	36	90	110	2.8	3.2	13.7	0.21 mg Mo
SS-5	7.0	3.0	0.33	57	1700	1900	0.0005	0.0013	14.0	0.34 mg Mo
HTSS-2	9.1	0.6	0.31	93	50	53	1.5	1.5	13.5	0.03 mg Mo
B-HTSS-2	8.4	0.8	0.46	90	47	52	1.5	1.6	13.5	—
HTSS-1a	14.4	2.7	0.40	81	53	54	1.8	1.6	13.5	0.001 mg Cr

mated from the amount of silica deposited according to Table 2, assuming homogeneous deposition on all exposed surfaces (surface area ~ 37 cm^2 for both modules). Accordingly, layer thicknesses amount to 42 µm (HTSS-2) and 56 µm (HTSS-1a).

From the data in Table 2 it may be concluded that high silica MFI (silicalite-1) is formed. Generally, no T atoms or other trivalent cations (Al, Fe, Cr), originating from the metal support and/or the silica source, are detected in either the synthesis gels or the supernatants (<0.2 ppm). Only some molybdenum (maximal concentration of 10 ppm) is detected in all analyzed supernatants, especially under more extreme conditions (SS-5; pH 14, 174 h). Under the assumption that the chemical compositions of the synthesis mixture and the MFI phase are equal, all Si/T ratios are higher than 5000. The concentration of alkali (Na, K) ions within the framework is also low. The explanation for the generally somewhat higher alkali concentrations in the supernatants (after synthesis) is attributed to the reduced liquid density, because substantial amounts of silica and TPA have been consumed for the crystallization. Due to the relatively low accuracy of the data presented in Table 2, only a maximal Si/Na ratio of 3000 can be given (assuming 10% error). The same holds for potassium, but as a result of the tenfold higher potassium concentration, the minimal Si/K ratio amounts to 300. It is, however, expected that hardly any potassium is present in the layer, because the incorporation of TPA in the MFI framework is strongly favoured.

From the low iron, nickel, and chromium concentrations in the supernatants, even for the high-temperature modules, the applied stainless steel

can be considered inert under the required hydrothermal synthesis conditions. This is also confirmed by experiment SS-5, which synthesis mixture was previously applied to prepare continuous MFI layers on ceramic supports [18]. On inert zirconia substrates, large, separately grown crystals were formed only after five days, as is the case in experiment SS-5. The chemical composition of the synthesis mixture is not affected by the presence of the inert support, and the crystallization proceeds in a similar way as for large, single crystals of MFI, previously described by Jansen et al. [25].

From the blank experiments (MFI crystallization in the absence of stainless steel), however, it seems that the stainless steel does affect the crystallization process, both in a chemical and a physical sense. Similar to the high-temperature modules, the Teflon lining in contact with the crystallization liquid is covered by MFI material. Several open spaces, on the other hand, remain present (Fig. 9a), and from the inhomogeneous nature of the layer the crystallization is expected to proceed in subsequently occurring stadia (Fig. 9b). Initially, small and somewhat aggregated crystals are formed, which is attributed to the high supersaturation of the synthesis mixture, followed by the growth of a more continuous layer on top of these aggregated crystals. Figure 9c presents the bottom side of the layer (facing the Teflon lining during hydrothermal synthesis) near one of the open spaces in the layer. Next to the open space, a rather dense MFI phase is formed, probably as a result of the second crystallization stadium. Finally, a top layer, similar to the one on the stainless steel support, is formed.

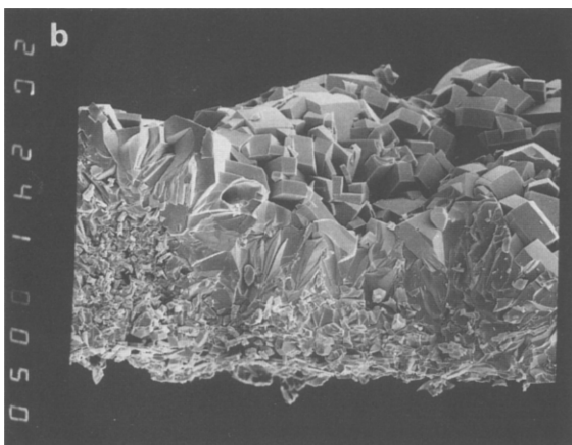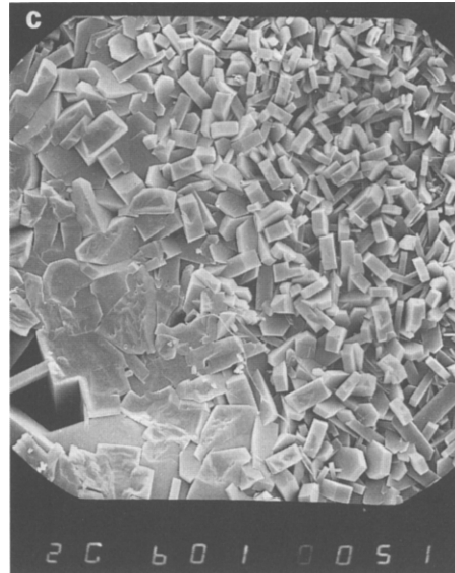The occurrence of large open spaces within the layer is attributed to the relatively poor adhesion
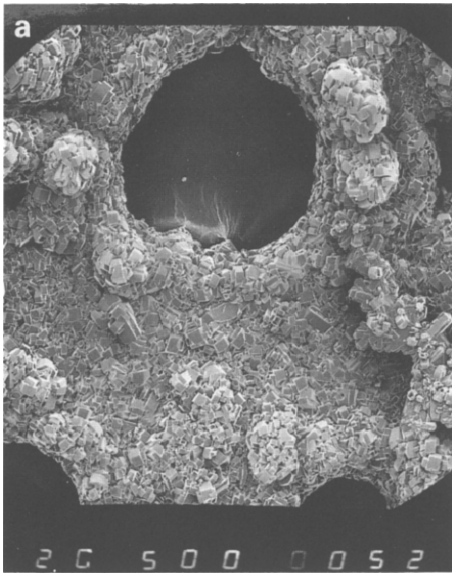
Fig. 9a. SEM picture of an unsupported MFI layer (top view), prepared according to B-HTSS-2 (magnification 50 ×).

Fig. 9b. Cross-sectional view of the same unsupported MFI layer, revealing its inhomogeneous nature (magnification 240 ×).

Fig. 9c. SEM picture of the bottom side of the same unsupported MFI layer, facing the Teflon surface during hydrothermal synthesis, near an open space (magnification 600 ×).

between the synthesis mixture and the hydrophobic Teflon surface (physical effect). In all experiments large amounts of TPA are introduced, and a high propene production due to the Hofmann degrada-tion reaction is expected [25]. The resulting vola-tiles (mainly propene and water) are concentrated in gas bubbles that adhere to the Teflon surface. Obviously, these gas bubbles hamper the formation

of a layer, fully covering the Teflon lining. The wetting of the hydrous solution to the more hydrophilic stainless steel, on the other hand, is excellent. Therefore, the gas bubbles produced are forced from the stainless steel support by the hydrous solution.

The presumed chemical effect is based on the fact that no small aggregated crystals are observed in the case of the stainless steel supported MFI layers. Apparently, the nucleation and crystal growth proceed in an essentially different manner on the stainless steel surface as compared with the inert Teflon lining. This may be caused by a local higher concentration of trivalent cations, such as Fe(III) and Cr(III), near the metal support. The occurrence of a dense silica gel phase, prior to the crystallization of cube-shaped single crystals of MFI has been attributed to the presence of low concentrations of trivalent cations [25]. Therefore, the stainless steel material is not expected to be fully inert, but the concentration of leached metal ions remains below the detection level of the chemical analysis. From the above considerations it may be argued that the present stainless steel supported, membraneous layer consists of randomly oriented MFI crystals, grown next to each other, similar to the previously reported ceramic (clay) supported MFI layers [18].

The relative inertness of the stainless steel material under the required hydrothermal conditions at high pH allows for recycling of the module. This compensates for the fact that rather complex modules have to be constructed, in order to achieve a high specific surface area. Upon removal of the calcined MFI layer from the membrane module (HTSS-1) by alkaline treatment, some leaching of iron, chromium, and molybdenum (<0.5 mg) has been observed. Less extreme conditions (0.5 M KOH; 180°C; 2 h) are expected to suffice to dissolve all silica within the module.

These results demonstrate that continuous, polycrystalline MFI layers can be prepared on inert stainless steel substrates, but the chemical composition of the synthesis mixture is restricted. In the first place, relatively thick (>10 μm) layers are required to achieve a complete coverage of the porous parts within the membrane module. Secondly, a rapid but homogeneous nucleation

and crystal growth should proceed on all (externally) exposed surfaces. A high TPA concentration within the synthesis gel is expected to enhance nucleation. In addition, TPA favours the growth of large MFI crystals. A relatively high SiO_2/OH^- ratio also gives rise to a high nucleation rate (high supersaturation), and moreover leads to an efficient use of the silica within the synthesis mixture for the formation of a continuous MFI layer. Therefore, the MFI membrane preparation according to HTSS-2 (high TPA concentration, cf. Table 1), is considered optimal. Further optimization of the membrane preparation, however, seems possible, for instance by varying the synthesis time and/or temperature, and may lead to another optimal gel composition.

Permeation

The as-synthesized metal supported MFI layers (HTSS-1, 2, and 1a) proved to be gas-tight (flow $<7.4 \cdot 10^{-12}$ mol/s; $P<4.1 \cdot 10^{-17}$ mol m m^{-2} s^{-1} Pa^{-1}) for a pure neon feed (100%), even after 1 h on stream. In Fig. 10 the pure gas (30% in helium) permeation behaviour of all gases through the calcined MFI layer (HTSS-2) is shown. The time to detect methane (34 s) and neon (38 s) is somewhat higher than the delay time of the experimental set-up (26 s). The detection of the butane fluxes depends strongly on the isomer: n-butane after 42 s, and isobutane after ~2 min. For methane, neon, and n-butane the steady state fluxes are
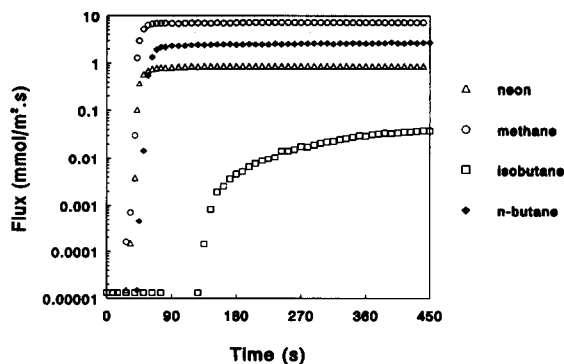

Fig. 10. Pure gas transient permeation behaviour (30% in helium; 1 bar total pressure) for methane, neon, n-butane, and isobutane at 25°C.

reached within 1–2 min. In the case of isobutane it takes over 10 min to reach steady state completely, and the permeation rate is 1–2 orders of magnitude lower. Under the applied conditions, the steady state permeabilities (in mol m m^{-2} s^{-1} Pa^{-1}) amount to $1.2 \cdot 10^{-11}$ (methane), $1.5 \cdot 10^{-12}$ (neon), $4.5 \cdot 10^{-12}$ (n-butane), and $7.0 \cdot 10^{-14}$ (isobutane).

The adsorption capacity of the membrane layer ($l_m = 50$ μm; $A_m = 3$ cm^2), assuming equilibrium under the applied conditions on the feed and the permeate side, and the observed steady state permeation rate may be combined to estimate the delay time to reach steady state permeation. Surprisingly, for methane and neon the estimates amount to only a few seconds, and are substantially lower than the actually required times. For n-butane, the estimated value is only somewhat lower (~1 min), whereas for isobutane the required delay time is substantially shorter than the estimated value (> 2000 s). Apparently, the transient permeation behaviour depends strongly on the permeating species. A more extensive comparison is published elsewhere [26].

In Table 3, the observed steady state flow rates for methane and n-butane are compared with the theoretical steady state permeation rates [21], according to the Fickian model in eqn (5). The observed flow rate for n-butane is of the same order of magnitude as the theoretical value, whereas for methane the experimental permeation rate is over one order of magnitude lower than the one according to theory. It is remarkable that the best agreement is found for n-butane, as the permeation model applied here is basically more reliable for methane, for which species adsorption remains within the Henry region.

In fact, somewhat lower experimental permeation rates are to be expected from the random orientation of the MFI crystals (vide supra). For only few crystals within the layer does the permeation proceed exclusively via the straight or sinusoidal channels so, due to the diffusional anisotropy [29], the average diffusivity through the MFI layer will be lower than maximal. The flow rate may be further reduced by the fact that some plugging of the stainless steel top layer by deposited MFI material occurred. Extra resistance to molecular flow by the presence of intercrystalline voids within the membraneous layer is, however, considered unlikely, because the crystals are grown separately next to, and not on top of each other.

The steady state permeation rates for methane and neon are not affected by the helium flow rate on the permeate side (variation 50–500 ml/min). Apparently, diffusion through the macroporous support does not affect the permeation rate. This has only been checked for the weakly adsorbing species [26], and as for near saturation adsorption the permeation rate depends on the partial pressure on the permeate side [21]. In fact, an intrinsic problem of the Wicke–Kallenbach approach is encountered here, because the permeate partial pressure and the flow rate through the membrane are interrelated. A higher purge gas flow rate on the permeate side leads to a lower permeate concentration, and a higher permeation rate is to be expected. The large difference in permeation rate between the two butane isomers is only partly attributable to the isobutane adsorption capacity of MFI, being only half the n-butane adsorption under the saturation conditions applied here [26,30]. According to permeation measurements on a twinned silicalite crystal at 24°C [7], the

TABLE 3

Comparison of methane and n-butane steady state permeation rates with the Fickian diffusion model, according to eqn. (5), for a feed of 30% sorbate in helium at 25°C

Gas	p_{feed} (kPa)	$p_{permeate}$ (kPa)	ϕ_{mol}(exp.) (mol s^{-1})	D_0[a] (m^2 s^{-1})	K[b] (mol m^{-3} Pa^{-1})	k[c] (Pa^{-1})	q_0[c] (mol m^{-3})	ϕ_{mol}(th.) (mol s^{-1})
Methane	30	2.9	$2.2 \ 10^{-6}$	$1.2 \ 10^{-8}$	0.0174	—	—	$3.3 \ 10^{-5}$
n-butane	30	1.1	$8.1 \ 10^{-7}$	$5.9 \ 10^{-9}$	—	$3.1 \ 10^{-2}$	$2.75 \ 10^{3}$	$2.5 \ 10^{-6}$

[a]Intrinsic diffusivity, parameter in the diffusion model [21], according to PFG NMR self-diffusion data from ref. 22. [b]Henry coefficient taken from ref. 27. [c]Langmuir isotherm parameters, fitted for adsorption data from ref. 28.

intrinsic diffusivity of isobutane is somewhat lower (by a factor of 3) than that of *n*-butane. Hence, the low permeation rate of isobutane as compared with *n*-butane under near saturation conditions (pure gas permeation ratio of over 60) may be attributed to the bulkiness of isobutane.

Typical transient permeation behaviour has been observed for a 50/50 methane/*n*-butane mixture (Fig. 11). The methane flux starts similar to the pure gas measurement in Fig. 10, but levels off after a few seconds to reach a temporary maximum. The permeation behaviour of *n*-butane is hardly affected by the presence of methane instead of helium on the feed side. Steady state is reached within 2 min, similar to the pure gas permeation experiment for *n*-butane. The selectivity (α), however, amounts to ~ 50 in favour of *n*-butane, whereas the ideal separation factor, based on pure gas permeabilities, is in favour of methane. In this case, separation is apparently governed by a difference in adsorption strength, and by the reduced mobility (*vide infra*) of methane within the zeolite micropores in the presence of strongly adsorbing molecules. Owing to the strong adsorption of *n*-butane, hardly any methane may enter the zeolite micropores, and the driving force for methane permeation is substantially reduced. On other supported MFI layers a similar but less pronounced behaviour of binary mixtures of weakly and strongly adsorbing molecules has been observed [21].

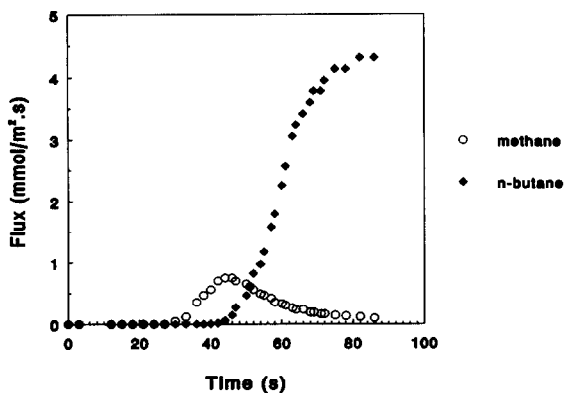The methane permeation is equally reduced in the presence of isobutane. In Fig. 12 the permeation behaviour of methane is shown, after either *n*-butane, or isobutane is added to the initially pure methane feed (70% in helium). Again, the required time to reach the new steady state depends on the butane isomer. The major drop in methane permeation, however, results directly after the feed gas has been switched, similar to *n*-butane. Even after short times, apparently, the zeolite micropores on the feed side are effectively blocked by the isobutane molecules. In spite of their different (pure gas) permeation behaviour, the methane permeation rate is of the same order of magnitude for both butane isomers. Based on the previously mentioned difference in sorption capacity, however, the methane sorbate concentration on the feed side may be higher in the presence of isobutane as compared with *n*-butane. Hence, a higher driving force for methane permeation is expected in the presence of isobutane, in principle leading to a higher methane permeation rate. Actually, the methane permeation rate in the presence of *n*-butane is even somewhat higher than for isobutane, which suggests that the higher driving force for methane permeation is cancelled by the presence of slow moving isobutane molecules. It was established by the PFG NMR method that in the presence of virtually immobile benzene molecules (2 per unit cell), the methane diffusivity within the MFI framework is reduced by approximately two orders of magnitude [31]. As for *n*-butane, all the methane molecules that enter the zeolite framework are dragged through

Fig. 11. Transient permeation behaviour of a binary methane/*n*-butane mixture at 25°C.
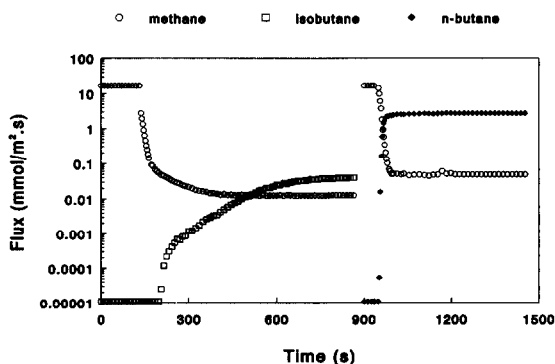

Fig. 12. Transient permeation behaviour for a methane feed (70% in helium), to which either *n*-butane or isobutane (30%) is added at 25°C.

the micropores by the fast moving n-butane molecules, and for both butane isomers at room temperature the high intrinsic mobility of methane is overruled.

The permeation behaviour (steady state) of a 50/50 methane/n-butane mixture (pure) as a function of temperature is shown in Fig. 13. A steady increase of the n-butane flux is observed (up to $\sim 160°C$). The methane permeation rate remains low up to $\sim 140°C$, and the selectivity is in favour of n-butane. At higher temperatures, the methane flow becomes substantial and even exceeds the decreasing n-butane flow at $\sim 230°C$. At still higher temperature (up to 350°C) the rise in methane permeation levels off. The same permeation behaviour for both gases is observed upon cooling, and has been found to be reproducible for several subsequent cycles. Thus, the metal supported MFI membrane remains thermomechanically stable up to at least 350°C.

All observed features in Fig. 13 may be related to the fact that both diffusion and adsorption are temperature dependent. For the n-butane permeation rate, the initial rise with temperature may arise from the higher intrinsic diffusivity, as diffusion is an activated process. Concurrently, however, the n-butane adsorption shifts out of the saturation area, first on the permeate side, so the driving force for n-butane permeation is also increased. For still higher temperatures, the driving force for n-butane decreases, as the adsorbate concentration on the feed side is no longer near

saturation. Still higher n-butane permeation rates may be reached by applying higher n-butane (partial) feed pressures.

For other than the feed conditions applied here (1 bar, 50/50 mixture), the permeation behaviour as a function of temperature may vary, although the trend is expected to be similar to Fig. 13. At low temperatures, the methane permeation rate is governed by the n-butane adsorbate concentration. The initial rise in methane permeation rate at low temperature may, therefore, be attributed to the increasing n-butane flow. At higher temperatures, the competition by the strongly adsorbing n-butane molecules diminishes, and both the driving force for methane permeation and the methane mobility are strongly increased. At sufficiently high temperatures, the selectivity is based on the pure gas permeability ratio (adsorption obeying Henry's law for both components) [26]. It should be noted that the true temperature dependency for the methane permeation, as presented in Fig. 13, is obscured by the presence of the n-butane molecules, whereas for n-butane, the presence of methane instead of helium is not expected to give rise to a significantly different permeation behaviour.

The strong blocking effect of n-butane and isobutane on the methane permeation under the conditions applied here (ambient conditions, p/p_0 ~ 0.14) shows that the membraneous layer consists of microporous material. These experiments do not, however, exclude the presence of larger pores, by which the separating potential of the membrane may be reduced. The presence of larger pores has been demonstrated by the fact that some transport of iso-octane takes place [26], which has no access to the MFI framework according to its molecular dimensions. The methane permeation is, however, hardly affected by the presence of iso-octane, whereas a comparable drop in the methane permeation is observed after the introduction of n-butane to the feed. Apparently, only few larger pores are present within the MFI layer, and their presence is not detrimental to the membrane performance.

To conclude, the permeation results presented here suggest that for mixtures consisting of weakly and strongly adsorbing molecules, the membrane is expected to be selective towards the latter, notwithstanding the generally lower intrinsic
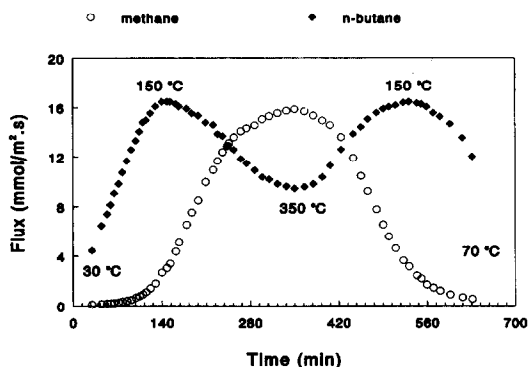

Fig. 13. Steady state permeation rates of a 50/50 methane/n-butane mixture as function of temperature (heating rate 1°C/min; cooling rate 1.5°C/min).

diffusivity for stronger adsorbing species. This type of membrane may, therefore, also be of interest to separate molecules with a difference in polarity. For example, the separation of water/ethanol mixtures on the silicalite-1 membranes reported here may lead to a substantial enrichment of ethanol, because the affinity of the hydrophobic MFI lattice for ethanol is much higher than for water [32]. The large difference in pure gas permeabilities of n-butane and isobutane, on the other hand, may not lead to high selectivities, as the difference in adsorption is only small.

Conclusions

Continuous polycrystalline membranes of MFI have been grown on two-layer porous, sintered stainless steel supports. High-temperature sealing is avoided by the formation of the zeolite layer on both porous and non-porous stainless steel parts. The incorporated TPA within the as-synthesized MFI phase can be removed by calcination in air at 400°C without the occurrence of cracks. In addition, no deterioration of the membrane performance has been observed after thermal cycling to 350°C.

High fluxes have been observed for small molecules, such as methane and neon, and linear alkanes (n-butane). For branched alkanes (isobutane) substantially lower fluxes are found. The diffusivities for methane and n-butane, based on the observed steady state permeation rates, are lower than the self-diffusivities according to the PFG NMR technique. Under conditions of near saturation adsorption, the selectivity is mainly governed by adsorption, favouring strongly adsorbing molecules over weakly adsorbing species.

Acknowledgements

References

1 H. Suzuki, US Pat. 4,699,892 (1987).
2 S. Sakurada, N. Tagaya, T. Maeshima and T. Isoda, Can. Pat. 1,235,684 (1988) to Toa Nenryo Kogyo Kabushiki Kaisha.
3 E.R. Geus, A. Mulder, D.J. Vischjager, J. Schoonman and H. van Bekkum, in A.J. Burggraaf, J. Charpin and L. Cot (Eds.), Key Engineering Materials, Vol. 61&62, Trans Tech Publications Ltd., Zürich, 1991, p. 57.
4 J.G. Tsikoyiannis and W.O. Haag, Zeolites, 12 (1991) 126.
5 F. Crea, R. Aiello, A. Nastro and J.B. Nagy, Zeolites, 11 (1991) 521.
6 T. Sano, Y. Kiyozumi, M. Kawamura, F. Mizukami, H. Takaya, T. Mouri, W. Inaoka, Y. Toida, M. Watanabe and K. Toyoda, Zeolites, 11 (1991) 842.
7 A.R. Paravar and D.T. Hayhurst, in D. Olson and A. Bisio (Eds.), Proc. 6th Int. Zeolites Conf., Butterworths, London, 1984, p. 217.
8 D.L. Wernick and E.J. Osterhuber, in D. Olson and A. Bisio (Eds.), Proc. 6th Int. Zeolites Conf., Butterworths, London, 1984, p. 122.
9 E.R. Geus, A.E. Jansen, J.C. Jansen, J. Schoonman and H. van Bekkum, Stud. Surf. Sci. Catal., 65 (1991) 457.
10 R.M. Barrer, J. Chem. Soc., Faraday Trans., 86 (1990) 1123.
11 R.M. Barrer, Stud. Surf. Sci. Catal., 65 (1991) 257.
12 J. Kärger and D.M. Ruthven, Zeolites, 9 (1989) 267.
13 H.P. Hsieh, Catal. Rev. Sci. Eng., 33 (1991) 1.
14 F.M. Velterop, Dutch Pat. Appl. 9,001,662 (1990).
15 C.E. Megiris, S.-W. Nam and G.R. Gavalas, in L. Cot and J. Charpin (Eds.), Proc. 1st Conf. Inorg. Membr., 1989, p. 355.
16 E. Wicke, Kolloid Z., 93 (1940) p. 9.
17 E. Wicke and R. Kallenbach, Kolloid Z., 97 (1941) 135.
18 E.R. Geus, M.J. den Exter and H. van Bekkum, J. Chem. Soc., Faraday Trans., 88 (1992) 3101.
19 M.F.M. Post, Stud. Surf. Sci. Catal., 58 (1991) 391.
20 L.S. Darken, Trans. AIME, 175 (1948) 184.
21 E.R. Geus, W.J.W. Bakker, P.J.T. Verheijen, M.J. den Exter, J.A. Moulijn and H. van Bekkum, in J.B. Higgins, R. von Ballmoos and M.M.J. Treacy (Eds.), Proc. 9th Int. Zeolites Conf., Butterworth–Heinemann, Stoneham, MA, 1992, accepted.
22 J. Caro, M. Bülow, W. Schirmer, J. Kärger, W. Heink, H. Pfeifer and S.P. Zdanov, J. Chem. Soc., Faraday Trans., 81 (1985) 2541.
23 M. Ghamami and L.B. Sand, Zeolites, 3 (1983) 155.
24 J.C. Jansen, W. Nugroho and H. van Bekkum, in J.B. Higgins, R. von Ballmoos and M.M.J. Treacy (Eds.), Proc. 9th Int. Zeolites Conf., Butterworth–Heinemann, Stoneham, MA, 1992, accepted.
25 J.C. Jansen, C.W.R. Engelen and H. van Bekkum, ACS Symp. Ser., 398 (1989) 257.
26 W.J.W. Bakker, E.R. Geus, G. Zheng, H. van Bekkum and J.A. Moulijn, in Conf. Proc. Precision Process Technology, October 27–29, 1992, Delft, Netherlands, Kluwer Academic Publ., accepted.
27 L.V.C. Rees, Stud. Surf. Sci. Catal., 65 (1991) 61.

28 R.E. Richards and L.V.C. Rees, *Langmuir*, 3 (1987) 335.
29 U. Hong, J. Kärger, R. Kramer, H. Pfeifer, G. Seiffert, U. Müller, K.K. Unger, H.B. Lück and T. Ito, *Zeolites*, 11 (1991) 816.
30 E.R. Geus and J.C.M. Muller, unpublished results.
31 J. Kärger, H. Pfeifer, D. Freude, J. Caro, M. Bülow and G. Ohlmann, *Stud. Surf. Sci. Catal.*, 28 (1986) 633.
32 W.-D. Einicke, M. Heuchel, M. v. Szombathely, P. Bräuer, R. Schöllner and O. Rademacher, *J. Chem. Soc., Faraday Trans.*, 85 (1989) 4277.